Cell

Dynamic Scaffolding in a G Protein-Coupled Signaling System

Prashant Mishra,[1,2,3] Michael Socolich,[1,2,3,4] Mark A. Wall,[1,2,3,4,5] Jennifer Graves,[1,2,3,6] ZiFen Wang,[1,2,3] and Rama Ranganathan[1,2,3,*]
[1]Howard Hughes Medical Institute
[2]The Green Center Division for Systems Biology
[3]Department of Pharmacology
University of Texas Southwestern Medical Center, Dallas, TX 75390-9050, USA
[4]These authors contributed equally to this work.
[5]Present address: Verenium Corporation, 4955 Directors Place, San Diego, CA 92121, USA.
[6]Present address: Department of Neurology, University of Pennsylvania, 3400 Spruce Street, Philadelphia, PA 19104-4283, USA.
*Correspondence: rama.ranganathan@utsouthwestern.edu
DOI 10.1016/j.cell.2007.07.037

SUMMARY

The INAD scaffold organizes a multiprotein complex that is essential for proper visual signaling in *Drosophila* photoreceptor cells. Here we show that one of the INAD PDZ domains (PDZ5) exists in a redox-dependent equilibrium between two conformations—a reduced form that is similar to the structure of other PDZ domains, and an oxidized form in which the ligand-binding site is distorted through formation of a strong intramolecular disulfide bond. We demonstrate transient light-dependent formation of this disulfide bond in vivo and find that transgenic flies expressing a mutant INAD in which PDZ5 is locked in the reduced state display severe defects in termination of visual responses and visually mediated reflex behavior. These studies demonstrate a conformational switch mechanism for PDZ domain function and suggest that INAD behaves more like a dynamic machine rather than a passive scaffold, regulating signal transduction at the millisecond timescale through cycles of conformational change.

INTRODUCTION

Proper subcellular localization of signal transduction proteins is critical for cellular information processing. One primary mechanism for localizing components is the use of scaffolding molecules—proteins that serve to bind and preorganize multiple members of a signaling pathway into macromolecular complexes (Bhattacharyya et al., 2006b). The importance of scaffolding has been demonstrated in several types of signaling pathways from diverse organisms (Morrison and Davis, 2003; Schoch et al., 2002; Wong and Scott, 2004), highlighting the generality of this mechanism in biology. By concentrating appropriate signaling proteins to local environments within cells, and thereby minimizing unwanted interactions, scaffolds are thought to optimize signaling efficiency, speed, and specificity.

Inactivation, no after-potential D (INAD), a *Drosophila* visual protein, has served as a prototypical model system for understanding scaffolding (Huber, 2001; Montell, 2005; Tsunoda and Zuker, 1999). Figure 1A shows a summary of the reactions organized by INAD. Visual transduction in *Drosophila* photoreceptor neurons takes place in a specialized organelle called the rhabdomere, a stack of roughly 30,000 microvilli within which INAD assembles several signaling proteins into a specific macromolecular complex (Hardie and Raghu, 2001). Signaling begins with the absorption of a photon of light by the G protein-coupled receptor rhodopsin and then proceeds via sequential activation of a Gq isoform of heterotrimeric G protein and a phospholipase C (the NORPA PLC-β) molecule to ultimately trigger the opening of cation-selective *T*ransient *R*eceptor *P*otential (TRP) channels in the microvillar membrane. Ca^{2+} influx then triggers both positive and negative feedback regulation that is essential for the extraordinary speed and sensitivity of invertebrate vision (Henderson et al., 2000; Ranganathan et al., 1991). The mechanism of Ca^{2+}-dependent positive feedback is yet unclear, but the negative feedback operates in part through activation of an eye-specific isoform of protein kinase C (eye-PKC) (Ranganathan et al., 1991; Smith et al., 1991). This visual signaling pathway has served as a general model system for G protein signaling; for example, the core components of the pathway (rhodopsin, Gq, PLC, PKC, and TRP) are now known to mediate various biological processes in organisms ranging from flies to mammals.

INAD plays an essential role in both activation and termination of the electrical response to light (Scott and Zuker, 1998; Shieh and Zhu, 1996; Tsunoda et al., 1997). INAD is a concatamer of five *P*ost-synaptic density 95,

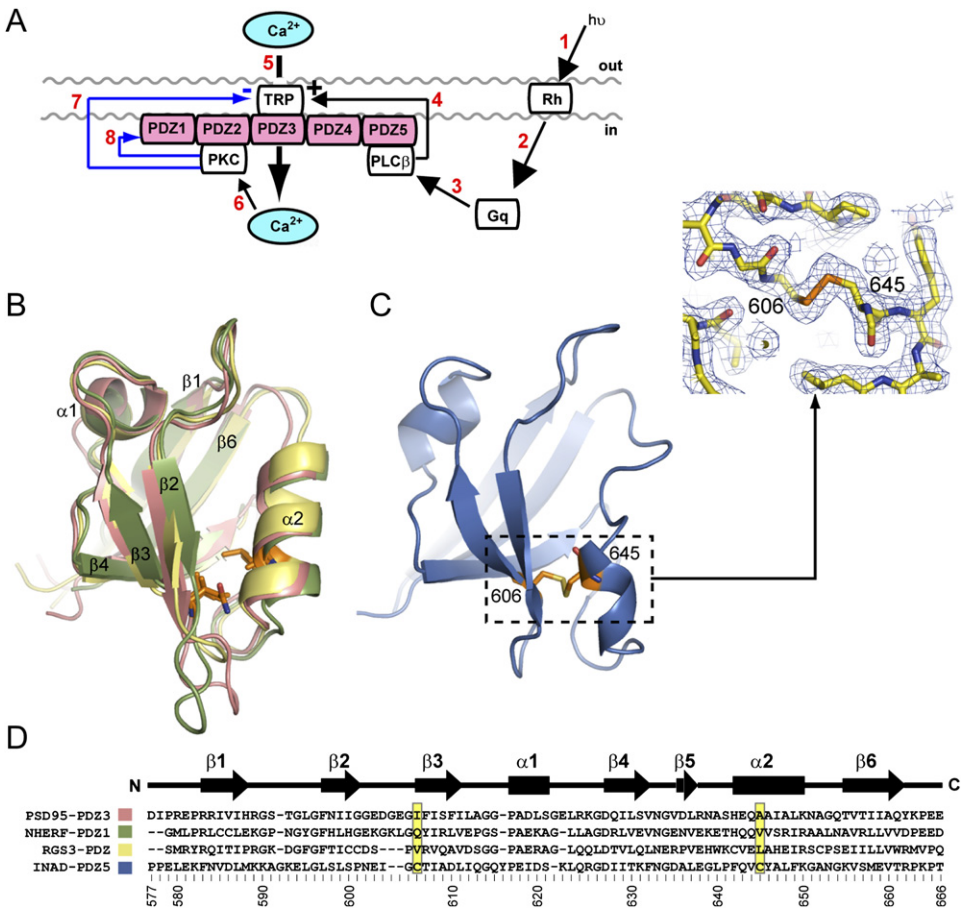

Figure 1. Scaffolding in *Drosophila* Vision

(A) Scaffolding in *Drosophila* vision. Photon absorption by rhodopsin (1) sequentially activates Gqα (2), PLC-β (3), and TRP cation channels (4). Calcium influx (5) activates an eye-specific kinase (eye-PKC, 6) which phosphorylates the TRP channel (7) and the INAD scaffold (in red, 8). Through its PDZ domains, INAD assembles a core macromolecular complex involving PLC-β, TRP, and eye-PKC.

(B) Structural overlay of three previously characterized PDZ domains (PDB codes 1BE9, 1G9O, and 2F5Y).

(C) The atomic structure of PDZ5 shows overall similarity in the β sheets, but significant conformational changes in both α helices (see Figure S1 for quantitation). Examination of the $2F_o - F_c$ electron density at 1σ indicates the presence of a disulfide bond between cysteines 606 and 645.

(D) Sequence alignment of the PDZ domains shown. The color code corresponds to the structures in (B) and (C); the positions of the two cysteines are highlighted in the alignment.

*D*iscs Large, *Z*ona Occludens 1 (PDZ) domains, a diverse and nearly ubiquitous family of protein interaction modules that bind the C-terminal residues of target proteins (Hung and Sheng, 2002). Through PDZ-mediated interactions, INAD assembles a core complex involving at least three proteins: the NORPA PLC-β (the main effector molecule for rhodopsin-mediated signaling), the TRP channel (the main mechanism of membrane depolarization and Ca^{2+} entry), and eye-PKC (the primary effector for Ca^{2+}-dependent negative feedback regulation) (Figure 1A) (Chevesich et al., 1997; Huber et al., 1996; Shieh et al., 1997; Tsunoda et al., 1997). The scaffolding of PLC-β to the INAD complex is critical for maintaining the high efficiency and speed of visual signaling (Scott and Zuker, 1998), and scaffolding of eye-PKC directs feedback phosphorylation reactions within the complex that are required for fast response termination (Henderson et al., 2000; Popescu et al., 2006).

Like INAD, many scaffolding proteins colocalize activation and feedback regulation processes, allowing for tight spatial and temporal control over signaling events (Bauman et al., 2006; Bhattacharyya et al., 2006a). This raises the possibility that conformational changes in scaffolding proteins during signaling events might represent one mechanism for dynamically modulating output responses. Here, we present crystallographic and functional evidence that the fifth PDZ domain of INAD undergoes a redox-dependent conformational switch that dramatically reorganizes the binding pocket. Light stimulation triggers this conformational switch in vivo, and physiological analysis shows that the switch is critical for shaping the visual response. These results demonstrate that INAD is

a dynamic scaffold, actively participating on the timescale of visual signaling through cycles of stimulus-dependent conformational change.

RESULTS

Structural Analysis of INAD PDZ5

As part of an overall study to structurally characterize INAD, we screened many constructs containing individual and multiple PDZ domains for expression and crystallization. Well-diffracting crystals of INAD PDZ5 (residues 580–665, hereafter called PDZ5) grew in space group $P4_12_12$ with two molecules per asymmetric unit (ASU). The structure was solved by multiple isomorphous replacement with anomalous scattering (MIRAS) and was refined to 2.05 Å resolution ($R = 22.4\%$, $R_{free} = 24.2\%$) with excellent stereochemistry (see Table S1 in the Supplemental Data available with this article online). PDZ domains are 90–100 amino acid modules that adopt a six-stranded β sandwich configuration with two flanking α helices (Figure 1B). Target C-terminal ligands bind in a surface groove formed between the β2 strand and α2 helix and make a number of interactions that determine both general and sequence-specific recognition (Doyle et al., 1996; Hung and Sheng, 2002). Both the overall three-dimensional (3D) structure and most details of ligand recognition are highly conserved in the family despite considerable sequence divergence (Figures 1B and 1D). Comparison of PDZ5 with several other PDZ structures revealed that, as expected, this domain shares the basic topology and core architecture of the PDZ family (Figure 1C). However, there are two major structural differences that make PDZ5 unique: (1) the α1 helix is rotated nearly 70° relative to its position in other known PDZ structures, and (2) the α2 helix is unwound at its C-terminal end and displaced toward the β2 and β3 strands, leaving only a short stretch of helical structure at the entry to the ligand binding pocket. Because residues in α2 comprise major determinants of substrate recognition (Doyle et al., 1996; Hung and Sheng, 2002), this conformation of PDZ5 is inconsistent with the canonical mode of peptide binding in PDZ domains (see below).

An obvious hypothesis for explaining the distortions in the binding pocket is evident in the PDZ5 structure. An intramolecular disulfide bond covalently links a pair of buried cysteine residues located underneath the floor of the ligand-binding pocket (residues 606 and 645, S-S bond distance = 2.0 Å, Figure 1C). The bond connects the β3 strand with the α2 helix, suggesting that this interaction may be responsible for the distortions in α2. The analogous positions in other "normal" PDZ domains contain side chains that pack against each other within the core (Figures 1B and 1D), suggesting that the two cysteines in PDZ5 may be positioned at such high effective concentration that a very stable covalent interaction is possible. To examine this, we measured the standard redox potential of the disulfide bond in PDZ5 (Figure 2A). Cysteine reactivity of recombinant PDZ5 protein is probed with a maleimide derivative (AMS, see Experimental Procedures) that specifically labels free thiol groups, adding approximately 500 Da per thiol. Thus, the fraction reacting with AMS indicates the fraction of protein in the reduced state. PDZ5 shows no reactivity when incubated in buffer containing no reductant; this is the expected outcome if all PDZ5 molecules are in the oxidized state. However, equilibration with increasing concentrations of the reductant dithiothreitol (DTT) causes the protein to shift steadily to the reduced state. From these data, we calculate a standard redox potential of -425 ± 2 mV for disulfide formation in PDZ5 (Figure 2B), indicating that the bond is indeed extremely strong. By comparison, the reducing potential of the cytosolic environment of most cells is −230 to −300 mV (Hanson et al., 2004; Hwang et al., 1995; Keese et al., 1999; Ostergaard et al., 2004), providing an initial hint that the PDZ5 disulfide may be present under physiological conditions in vivo.

To structurally characterize the reduced state of PDZ5, we recrystallized the protein in the presence of 10 mM DTT—a condition under which we expect a reasonable fraction of both reduced and oxidized species. Crystals now grew in a different space group ($P4_322$) with three molecules per ASU. The structure was solved by selenomethionine multiwavelength anomalous dispersion (MAD) methods, and refined to 2.2 Å resolution ($R = 20.6\%$, $R_{free} = 23.1\%$, Table S2), without use of noncrystallographic symmetry restraints. Remarkably, we find that each of the three molecules in the ASU represents a distinct structural state for PDZ5 (Figure 2C). One molecule (blue, Figures 2C and 2D, S-S bond distance = 2.1 Å) is in the same oxidized state as in the original structure and shows the same distortions in the α1 and α2 helices described above. In contrast, the green molecule (Figures 2C and 2E, S-S distance = 3.8 Å) is in the reduced state; examination of the $2F_o - F_c$ electron density clearly shows that the disulfide bond is broken. In the reduced state, the α1 helix remains in the unusual rotated conformation, but the structure of the α2 helix is returned to the canonical form found in all PDZ domains (compare Figures 1B and 2E, and for quantitation, Table S4 and Figure S1). Like the green molecule, the red molecule (Figures 2C and 2F, S-S distance = 3.7 Å) is also in the reduced state but shows an extra unexpected feature: the C-terminal region of the neighboring blue protomer is coordinated within its ligand-binding pocket. Most likely, this interaction is a consequence of high local concentration of a terminal carboxylate-containing sequence rather than physiologically meaningful, but it suggests that the reduced state of PDZ5 is capable of binding ligands at the same surface groove as other PDZ domains.

A quantitative comparison of the different PDZ5 structures reveals that there are no significant differences between the oxidized and reduced states outside of the α2 helix (all atom rmsd for α2 = 2.16 Å; for all other residues = 0.65 Å). Even in the binding pocket, residues contributed by the β2 strand (K590, L595, L597, S598, and L599) are unaffected by the conformational switch, but

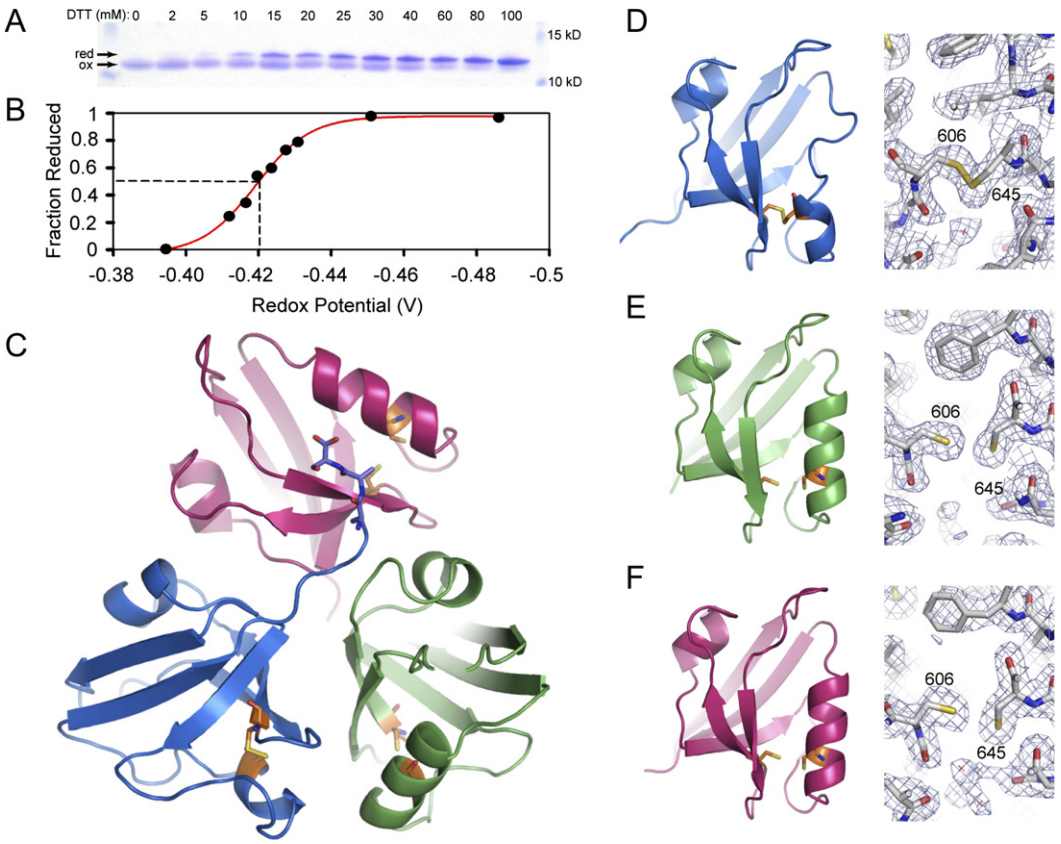

Figure 2. A Structure of INAD PDZ5 under Reducing Conditions

(A) A cysteine reactivity assay using a small maleimide reagent (~500 Da added per free thiol) shows that PDZ5 titrates into a reduced form upon incubation with the reducing agent dithiothreitol (DTT).

(B) A plot of the fraction reduced as a function of environmental redox potential is well fit by a two-state equilibrium model.

(C) The atomic structure of PDZ5 in 10 mM DTT reveals three molecules in the asymmetric unit, each of which is structurally distinct.

(D–F) (D)–(F) show each monomer with the corresponding electron density ($2F_o - F_c$, contoured at 1σ) in the region of C606 and C645. One molecule is in the oxidized state (D), one molecule is in the reduced state (E), and one molecule is in the reduced state with the C-terminal region of a neighboring molecule in the putative binding pocket (F).

key specificity-determining residues from the α2 helix (F642 and F649) adopt distinct conformations (Figure 3A). The α2 positions in the reduced state are consistent with known binding modes for PDZ domains (Doyle et al., 1996; Hung and Sheng, 2002) (Table S4). Thus, PDZ5 can exist in equilibrium between two structural states—an oxidized state in which the ligand-binding pocket is specifically distorted through formation of the C606-C645 disulfide bond, and a reduced state in which the pocket is in the canonical geometry for all PDZ domains (Table S4).

To independently test the idea that disulfide formation is causally linked to the conformational changes, we perturbed the bond by a cysteine to serine mutation at position 645. Crystals of $PDZ5^{C645S}$ grew in the absence of DTT in space group $P4_332$ with two molecules per ASU, and the structure was solved by selenomethionine single wavelength anomalous dispersion (SAD) methods and refined to 1.55 Å resolution (R = 24.8%, R_{free} = 26.7%, Table S3). The structure of $PDZ5^{C645S}$ is quantitatively indistinguishable from that of the reduced state of PDZ5 (all-atom rmsd of 0.96 Å, Figure 3B and Figure S1), indicating that the disulfide bond is necessary to switch the α2 helix into the distorted conformation. In addition, $PDZ5^{C645S}$ shows similar stability as the reduced form of the wild-type protein (Figure S2C), consistent with the model that the C645S mutation locks PDZ5 in the reduced state without causing significant neomorphic effects.

Light-Dependent Dynamics of the PDZ5 Disulfide In Vivo

To characterize the disulfide-mediated conformational switch in vivo, we constructed transgenic flies expressing either a wild-type copy of INAD or the C645S mutant under the control of a photoreceptor-specific promoter in an INAD null ($inaD^1$) genetic background ($yw;inaD^1;P[inaD^{WT}]$ and $yw;inaD^1P[inaD^{C645S}]$, hereafter called $inaD^{WT}$ and $inaD^{C645S}$, respectively; details on the fly stocks used

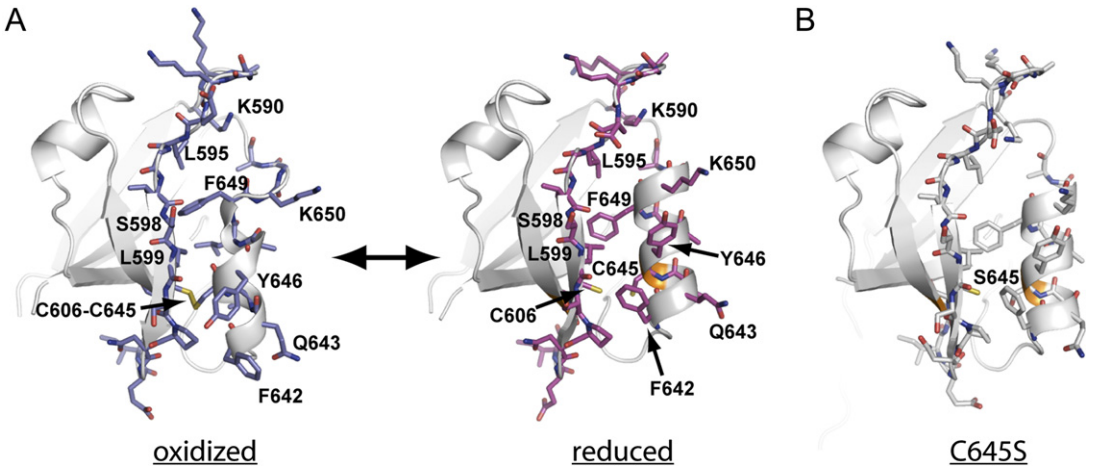

Figure 3. A Two-State Model for INAD PDZ5

A detailed view of the binding pocket in oxidized and reduced states of INAD PDZ5 (A) and in the C645S mutant structure (B). Key specificity-determining residues (F642 and F649) on the α2 helix adopt significantly different conformations in the oxidized and reduced states; the C645S mutant is effectively locked in the reduced state structure.

are presented in the Supplemental Experimental Procedures). Transgenic lines showed normal expression levels of both wild-type and C645S mutant INAD in vivo (Figure S2A).

To assay for disulfide formation in vivo, we developed a method modified from earlier work on monitoring thiol-disulfide interconversions in bacteria (Leichert and Jakob, 2004). In short, dissected retinas were directly homogenized into a 25% trichloroacetic acid solution to precipitate all proteins and instantly capture their native redox state, followed by a two-step maleimide reactivity assay (Figure 4A). Under denaturing conditions, resolubilized proteins are first reacted with a maleimide (AMS) to block all free thiols, then subjected to disulfide reduction, and finally reacted with a fluorescently labeled maleimide (Cy3m). After 2D gel electrophoresis of total protein, Cy3 detection allows the specific visualization of disulfide bond-containing proteins (Figures S3A–S3C).

We compared the pattern of Cy3-labeled proteins in dark-reared and light-exposed flies. Light exposure in wild-type animals causes the appearance of a series of spots at a mobility of ~85 kDa and a pI range of 5–8 (Figures 4B and 4C, full gels are in Figure S4), parameters consistent with a multiply phosphorylated INAD species (Figure S3C). These spots are specifically missing in both INAD null (Figure 4E) and *inaD*^{C645S} transgenic animals (Figure 4F), are recovered in *inaD*^{WT} transgenic animals (Figure 4G), and are recognized by an INAD-specific antibody (Figure S3C), strongly suggesting (1) that the spots are indeed INAD, and (2) that the disulfide detected is the C606-C645 interaction. Exposure of wild-type animals to light followed by a half-hour of dark adaptation causes the spots to disappear (Figure 4D), indicating that the PDZ5 disulfide is transient—forming upon light exposure and relaxing back to the reduced state when the cell is returned to the dark. To independently confirm these results, we directly monitored INAD's mobility on a nonreducing 1D gel, obtaining similar results and confirming that the disulfide bond is not intermolecular (Figure S3D). Thus, INAD cycles between these two states in vivo in response to light stimuli.

Mutant flies that lack the major rhodopsin of the compound eye (*ninaE*^{I17}) show greatly reduced Cy3m labeling of INAD (Figure 4H) though total levels of INAD are unaffected (Figure S2B), suggesting that PDZ5 disulfide formation is dependent on activation of the phototransduction cascade. (Residual labeling is expected due to expression of minor rhodopsin isoforms [Iakhine et al., 2004].) The mechanism downstream of rhodopsin that triggers this transition is yet unknown, but one obvious hypothesis implicates eye-PKC, the component of the INAD complex that mediates light-dependent feedback regulation. Known substrates of eye-PKC include the TRP channel and INAD itself (Matsumoto et al., 1999; Popescu et al., 2006); thus, phosphorylation of INAD could represent the signal by which light shifts the equilibrium of the C606-C645 disulfide. Light exposure fails to trigger proper formation of the INAD disulfide bond in *inaC*^{209} mutants (Figure 4I) despite wild-type levels of INAD (Figure S2B), providing an initial clue that eye-PKC activity may control INAD conformational dynamics. This result motivates a thorough mapping and characterization of the multiple eye-PKC phosphorylation sites on INAD.

A Light-Dependent Inactivation Defect in *inaD*^{C645S} Cells

To understand the functional role of the PDZ5 disulfide bond in vivo, we used whole-cell voltage clamp recordings in isolated wild-type and *inaD*^{C645S} mutant photoreceptor cells to measure their electrical responses to light. Wild-type photoreceptors respond to single photons by

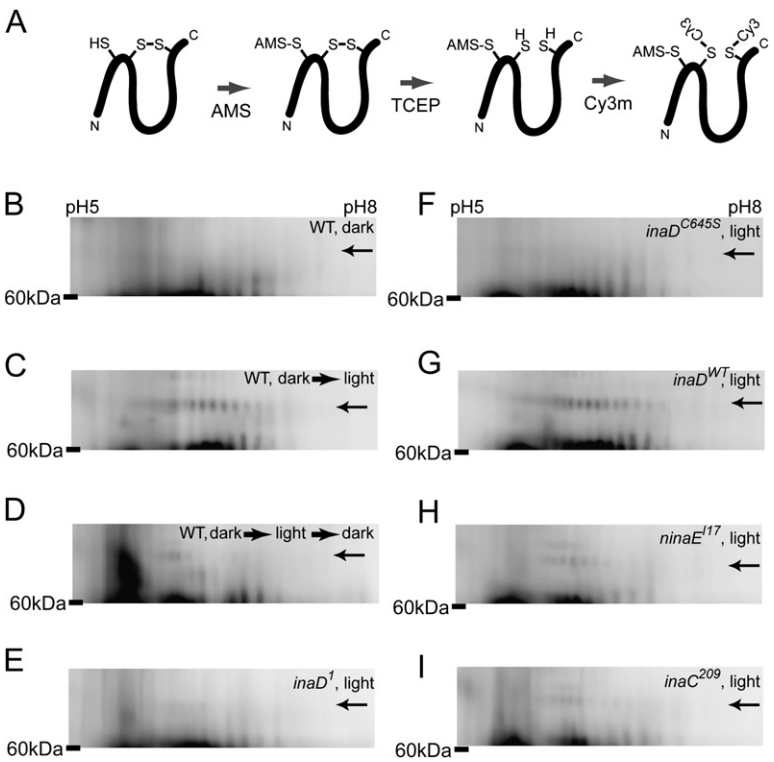

Figure 4. INAD PDZ5 Disulfide Formation In Vivo

(A) Schematic for specific labeling of disulfide bond-containing proteins. Free cysteines are first blocked with the maleimide reagent (AMS); any disulfide bonds are then reduced with the reductant (TCEP) and labeled with the fluorescent reagent, Cy3 maleimide (Cy3m).

(B–I) 2D gels of disulfide-containing proteins from dark-reared wild-type flies (B), light-exposed wild-type flies (C), light-exposed wild-type flies returned to the dark (D), light-exposed INAD null flies (*inaD*^{1}) (E), light-exposed *inaD*^{C645S} flies (F), light-exposed *inaD*^{WT} flies (G), light-exposed *ninaE*^{I17} flies that are null for the major rhodopsin of the eye (H), and light-exposed *inaC*^{209} flies that are null for eye-PKC (I). The position of the labeled INAD species is indicated by the arrows. Full gels are in Figure S4, and image intensities are normalized for total protein levels.

producing transient all-or-nothing electrical responses known as quantum bumps, which are thought to represent the coordinated opening of TRP channels in an individual microvillus and are summed to produce the macroscopic response to brighter stimuli (Henderson et al., 2000). Quantum bumps provide a sensitive measure of INAD function; mutants that impair its ability to bind TRP, eye-PKC, or PLC-β display severe defects in various bump properties (Henderson et al., 2000; Scott and Zuker, 1998). Wild-type quantum bumps are ~10 pA in magnitude and occur with a variable time delay (or "latency") (Figure 5A) (Hardie and Raghu, 2001). In the recording conditions used here, wild-type cells show a mean latency of about 50 ms. PDZ5 function is critical for this fast average response time; a point mutation in PDZ5 that specifically abrogates the interaction of INAD with the NORPA PLC-β (the *inaD*^{2} allele [Tsunoda et al., 1997]) shows normal quantum bump shape and amplitude, but a dramatically lengthened latency (Figure 5B) (Scott and Zuker, 1998). These mutants are thus capable of producing quantum bumps but are unable to organize them in time to produce significant and fast macroscopic responses. As expected, *inaD*^{WT} photoreceptors show normal quantum bumps (Figure 5C), consistent with full rescue of this phenotype. Interestingly, we find that *inaD*^{C645S} mutants show entirely wild-type quantum bump shape, latency, and amplitude (Figures 5D–5G). In addition, *inaD*^{C645S} mutants also show the same stimulus threshold for quantum bump production as wild-type cells (Figure 5H), indicating normal sensitivity to light. In short, *inaD*^{C645S} photoreceptors are completely normal in their ability to produce and time quantum bumps. This finding is consistent with the crystallographic and biochemical evidence that PDZ5 is in the reduced state upon dark adaptation and that the C645S mutation simply locks the domain in this conformation. In addition, it implies that the mutant protein is not impaired in its ability to bind any of its core binding partners (TRP, PLC-β, and eye-PKC).

In contrast to the quantum bump results, severe defects appear in *inaD*^{C645S} mutants upon stimulation with brighter light flashes. At lower light levels (Figure 6A, top; $\log(I/I_0) = -2.0$, or ~100 absorbed photons per flash), the response from *inaD*^{C645S} photoreceptors is indistinguishable from wild-type and *inaD*^{WT} responses. Curiously, as the flash intensity is increased, an inactivation defect appears and becomes more pronounced in *inaD*^{C645S}, but not *inaD*^{WT}, cells (Figures 6A and 6B). Thus, the reduced state of PDZ5 supports normal visual function at low-light levels, but transition to the oxidized state is necessary within milliseconds of rhodopsin activation in order to maintain fast shutoff during responses to physiologic stimuli.

A Specific Defect in the Refractory Period Following a Quantum Bump

Defects in response inactivation have been documented in other *Drosophila* mutants; for example, loss-of-function mutations in arrestin (*arr2*^{3}), the inhibitor of activated rhodopsin, or eye-PKC (*inaC*^{209}) also show slow termination of macroscopic light responses (Dolph et al., 1993; Henderson et al., 2000; Ranganathan et al., 1991).

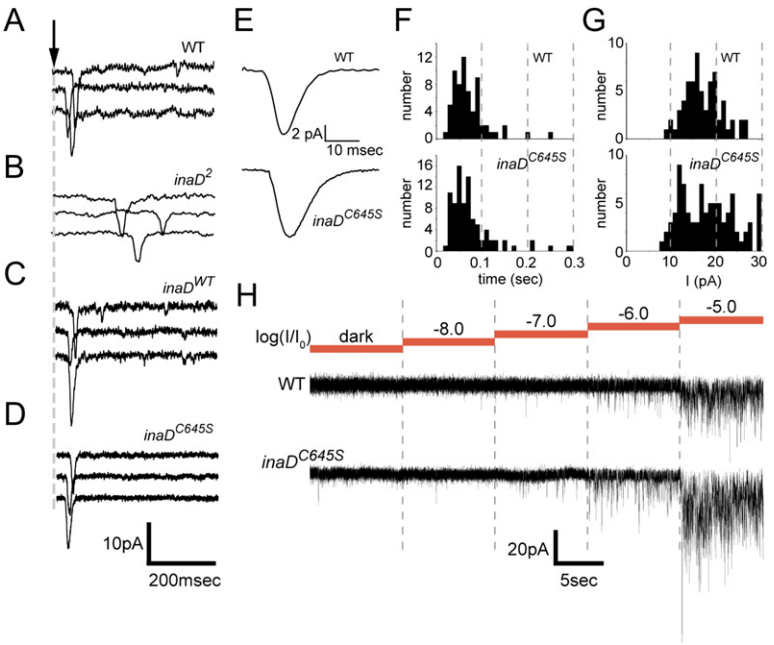

Figure 5. Single Photon Responses in *inaD*^{C645S} Cells

(A–D) Representative quantum bumps from wild-type photoreceptors (A), *inaD*^{2} photoreceptors (B), *inaD*^{WT} photoreceptors (C), and *inaD*^{C645S} photoreceptors (D). Time of photon delivery is indicated by the arrow.

(E–G) (E) Quantitative analysis of the average quantum bump shape (E), latency distribution (F), and amplitude distribution (G) from wild-type and *inaD*^{C645S} photoreceptors shows no significant differences in any of these properties.

(H) Stimulus thresholds for quantum bump production in wild-type and *inaD*^{C645S} photoreceptors. Dark-adapted cells are challenged with consecutively increasing amounts of light. Both genotypes consistently produce quantum bumps at the same stimulus intensity ($\log[I/I_0] = -6.0$; I is the stimulus intensity; I_0 is the [reference] intensity of the unattenuated laser).

However, these defects are evident at all light intensities including at the single photon limit, suggesting that the mechanism underlying the *inaD*^{C645S} phenotype is fundamentally different.

To understand the defect in *inaD*^{C645S} cells, we examined the average size, shape, and rate of production of quantum bumps as a function of increasing stimulus intensity. Individual bumps cannot be resolved during multiphoton stimuli, but average properties of the quantum bumps underlying steady-state macroscopic responses can be extracted using stationary fluctuation analysis (see Experimental Procedures) (Juusola and Hardie, 2001; Wong and Knight, 1980; Wu and Pak, 1978). As expected, wild-type photoreceptor cells show a classical adaptation response in which both quantum bump amplitude and duration decrease steadily as the stimulus intensity increases (Figures 6C and 6D, black traces) (Burack and Shaw, 2000; Johnson and Pak, 1986; Juusola and Hardie, 2001). These adjustments allow photoreceptors to extend the dynamic range of vision over several log orders of stimulation without saturation. *inaD*^{C645S} mutants are indistinguishable from wild-type in these parameters (Figures 6C and 6D, red traces), indicating that conformational switching in PDZ5 plays no role in classical light adaptation.

In contrast, a clear defect emerges in the rate of production of quantum bumps (Figure 6E). At low stimulus intensity, the bump rate rises linearly with a slope close to unity in both wild-type and *inaD*^{C645S} photoreceptors (Figure 6E, solid black and red lines). This is the expected outcome when each photon stimulates a distinct microvillus and quantum bumps are produced independently. However, at higher light intensities at which multiple photons would be absorbed by individual microvilli, the bump rate in wild-type cells rises with a shallower slope (Figure 6E, dashed black line), indicating that some mechanism limits the rate of bump production to less than the rate of incoming photons. Strikingly, bump rates in *inaD*^{C645S} mutants continue to rise unattenuated for the entire range tested (Figure 6E, red line).

These data indicate that defining the *inaD*^{C645S} phenotype begins with understanding why the bump rate levels off in wild-type cells when multiple rhodopsins are activated in an individual microvillus. An experimental approach for addressing this question is suggested by previous work on hypomorphic mutants of arrestin (*arr2*^{3}) and calmodulin (*cam*) (Scott et al., 1997). Both these mutants are severely defective in the shutoff of activated rhodopsin; thus, single photon stimulation leads to persistent signaling activity that approximates a continual stream of incoming photons into one microvillus. As demonstrated, the quantal response in these mutants is not a merely a single bump with broad kinetics. Instead, it consists of a normal shaped initial bump followed by a series of irregularly timed subsequent responses that have been referred to as a "bump train" (Figure 6F) (Hardie, 2001; Hardie and Raghu, 2001; Scott et al., 1997). The key feature of this phenotype is the existence of a refractory period following an individual quantum bump during which channel activity is silenced in the activated microvillus. However, the mechanistic basis for the refractory period is unknown.

These findings suggest a straightforward hypothesis for the *inaD*^{C645S} phenotype. By definition, the maximum bump rate for any wild-type microvillus is limited to once per refractory period. Thus, at stimulus levels that are high enough to yield a reasonable probability that microvilli receive multiple photons within a refractory period,

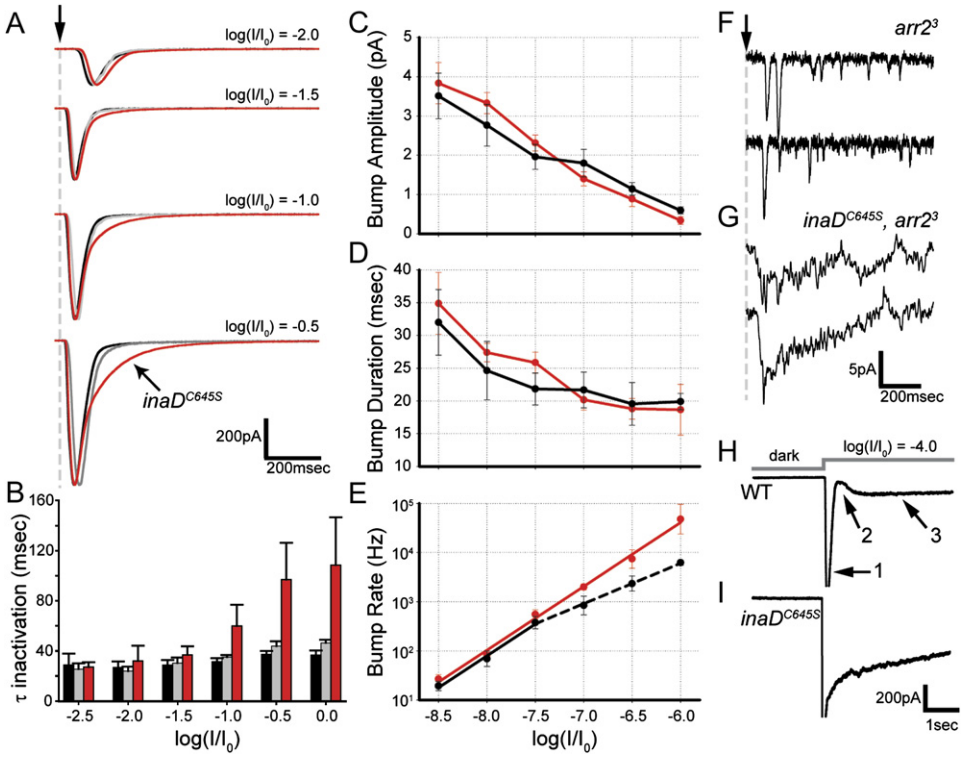

Figure 6. Light-Dependent Inactivation Defects in *inaD*^{C645S} Cells

(A) Average macroscopic responses from wild-type (black), *inaD*^{WT} (gray), or *inaD*^{C645S} (red) to 3 ns flashes of 580 nm laser light at the indicated intensities. Responses are normalized to peak at each light intensity, and I_0 is the (reference) intensity of the unattenuated laser (~10^4 absorbed photons).

(B) Time constants obtained from fitting the inactivation segments of macroscopic responses to a single exponential. Error bars indicate standard deviations, and the color scheme is the same as in (A).

(C–E) Stationary fluctuation analysis was used to measure average bump amplitude (C), duration (D), and rate (E) as a function of light intensity in wild-type (black) and *inaD*^{C645S} (red) photoreceptors. Bars indicate standard errors. Here, I_0 is the reference intensity of the unattenuated lamp.

(F and G) Representative single photon responses from *arr2*^{3} (F) and *inaD*^{C645S}, *arr2*^{3} photoreceptors (G) confirm that *inaD*^{C645S} mutants have a near complete loss of the refractory period between sequential quantum bump events.

(H and I) Electrical responses from dark-adapted wild-type (H) and *inaD*^{C645S} (I) photoreceptors suddenly stimulated with constant light at the indicated time and intensity reinforce this conclusion (see text).

we expect the leveling off of bump rates observed in wild-type cells (Figure 6E, black line). Given this, the unattenuated production of quantum bumps observed in *inaD*^{C645S} animals (Figure 6E, red line) suggests a dramatically shortened (or even absent) refractory period. To test this, we recorded from *inaD*^{C645S}, *arr2*^{3} double mutant animals (*yw; inaD*^{1}*P[inaD*^{C645S}*]; arr2*^{3}). If the refractory period is absent, then the combination of these two mutations should transform the *arr2*^{3} bump train into just a continuously decaying quantum bump. Figure 6G confirms this prediction, supporting the model that the fundamental physiological defect in *inaD*^{C645S} mutants is selective abrogation of the refractory period following a quantum bump.

Direct observation of the refractory period in wild-type cells under conditions of brighter, constant light stimulation is difficult, as the electrical responses from different microvilli are not matched in time. Thus, the steady-state macroscopic response represents the sum of many unsynchronized quantum bump trains from different microvilli. However, synchronization can be transiently achieved by instantly shifting cells from darkness to bright light (Figure 6H). By using a shutter with an opening time (~8 ms) that is significantly faster than the average latency for bumps (~50 ms, Figure 5F), we expect that the initial responses and refractory periods from an ensemble of microvilli will occur approximately simultaneously. This synchronization is not expected to last for long; the random nature of the refractory periods between quantum bumps (Figure 6F) will cause rapid decorrelation of the responses from different microvilli as time progresses. Accordingly, wild-type cells show an initial transient channel opening (Figure 6H, arrow 1), followed by a dip in activity (arrow 2) that then progresses to a constant steady-state current (arrow 3). *inaD*^{C645S} animals show no dip in channel activity (Figure 6I). These data strongly suggest (1) the existence of a refractory period in wild-type photoreceptor cells under physiologic conditions

and (2) that $inaD^{C645S}$ mutants have specifically lost the refractory period between quantal responses.

Taken together with the structural and biochemical data, these findings allow us to propose a simple mechanistic model: the reduced conformation of PDZ5 defines a permissive condition for signaling, and the oxidized conformation defines the refractory period. From a dynamic perspective, this model argues that INAD cycles between these states on the hundreds of milliseconds timescale of the visual response.

Consequence of Refractory Period Loss

Loss of the refractory period clarifies one yet unexplained aspect of the $inaD^{C645S}$ phenotype—the intensity-dependent inactivation defect observed in macroscopic flash responses (Figure 6A). For low intensity flashes, each microvillus very rarely receives multiple photons. Thus, loss of the refractory period has no consequence and $inaD^{C645S}$ mutants show no defects (Figure 6A, top panel). As stimulus intensity increases, multiple rhodopsins will be activated per microvillus and now the refractory period becomes of functional significance. Rhodopsin activation will still produce an initial quantum bump with normal latency and shape; however, without a refractory period, signaling from other simultaneously activated rhodopsins would be expected to stimulate additional quantum bump responses in the period before they are shut off. Integrated over many microvilli, such responses would produce a slow inactivation of the macroscopic response (Figure 6A, lower panels). Thus, as suggested (Hardie and Raghu, 2001), the refractory period allows signal shutoff to be determined "downstream"—by rapid channel inactivation rather than by potentially slower events such as arrestin binding and GTPase activity.

What is the consequence of loss of fast inactivation of the light response for fly vision? At the cellular level, one well-known phenotype is the inability to rapidly reset photoreceptor sensitivity following a bright (but physiological) stimulus (Smith et al., 1991); the excess signaling activity presumably either overdrives adaptation mechanisms or depletes excitatory intermediates. $inaD^{C645S}$ cells share this phenotype (Figures 7A and 7B); mutant photoreceptors are unable to restore and maintain sensitivity following sudden changes in light levels, indicating that transient formation of the PDZ5 disulfide is critical for maintaining responsiveness in the face of bright stimuli.

However, a more profound phenotype is evident at the behavioral level. Because motion sensing by visual processing centers in the fly brain requires well resolved photoreceptor responses in the compound eye (Franceschini et al., 1981), the broadening of response kinetics in $inaD^{C645S}$ flies should significantly degrade the ability of animals to respond to visual cues. For instance, *Drosophila* have evolved specialized reflex circuits that trigger escape behavior in response to specific visual cues. In response to the expanding shadow over the retina produced by an approaching predator, the giant fiber neuron (receiving input from visual fibers) activates muscles in the legs and thorax, producing an escape jump and flight behavior (Holmqvist and Srinivasan, 1991; Wyman et al., 1984). The behavior can be reliably evoked in the laboratory by rapid shutoff of ambient light (Movie S1); in response to a 20 ms "lights-off" stimulus, wild-type and $inaD^{WT}$ flies jump ~70% of the time (Figure 7C). In contrast, $inaD^{C645S}$ flies have a dramatic defect in escape behavior (jumping only 10% of the time, Movie S2, Figure 7C), indicating that they are unable to sense sudden decreases in light intensity. The phenotype is specific to the ability to rapidly deactivate the light response, as mutant animals show no defects in phototaxis behavior, or escape behavior due to a mechanical stimulus (also mediated by the giant fiber system) (Figure 7C). Thus, the refractory period, via its effect on maintaining rapid deactivation of the light response, plays a critical role in an evolutionarily conserved escape behavior.

DISCUSSION

Conformational Dynamics in the INAD Scaffold

Previous work on INAD has established the concept of a "transducisome" (Tsunoda et al., 1997) or "signalplex" (Montell, 1998)—essentially a preordered macromolecular complex that carries out a series of signaling reactions with great speed and specificity. We extend this concept by showing that INAD is a dynamic scaffold, undergoing cycles of intramolecular disulfide bond formation in one PDZ domain. Crystallographic studies define this conformational switch at atomic resolution, and experiments both at the cellular and behavioral levels indicate a clear biological role for this process in maintaining fast timescale visual function. To our knowledge this work provides the first example of such large-scale conformational switching in the PDZ domain, and opens the possibility that other members of this large family of scaffolding modules may also be engaged in dynamic conformational changes.

The notion that redox chemistry plays a role in regulating the *Drosophila* visual system is not without precedent; the first PDZ domain of INAD (PDZ1) has been proposed to be involved in an intermolecular disulfide interaction with the C-terminal region of the NORPA PLC-β (Kimple et al., 2001). Specifically, a cocrystal structure of PDZ1 bound to the predicted C-terminal peptide of NORPA (NH_2-GKTEFCA-COOH) indicates a covalent interaction between C31 on PDZ1 and the cysteine at the penultimate position of the peptide (NORPA position 1094). However, further evidence argues that this structural finding, though technically accurate, is not physiological (Figure S5). C31 is not conserved in the INAD ortholog from the closely related fly *Calliphora vicinia* (Figure S5A), and genomic sequencing of the *norpA* gene both by us (Figure S5B) and by the *Drosophila* genome project (Celniker et al., 2002) indicates a sequencing error at position 1094 in the original report of the NORPA sequence (Bloomquist et al., 1988); the cysteine reported at this site is actually

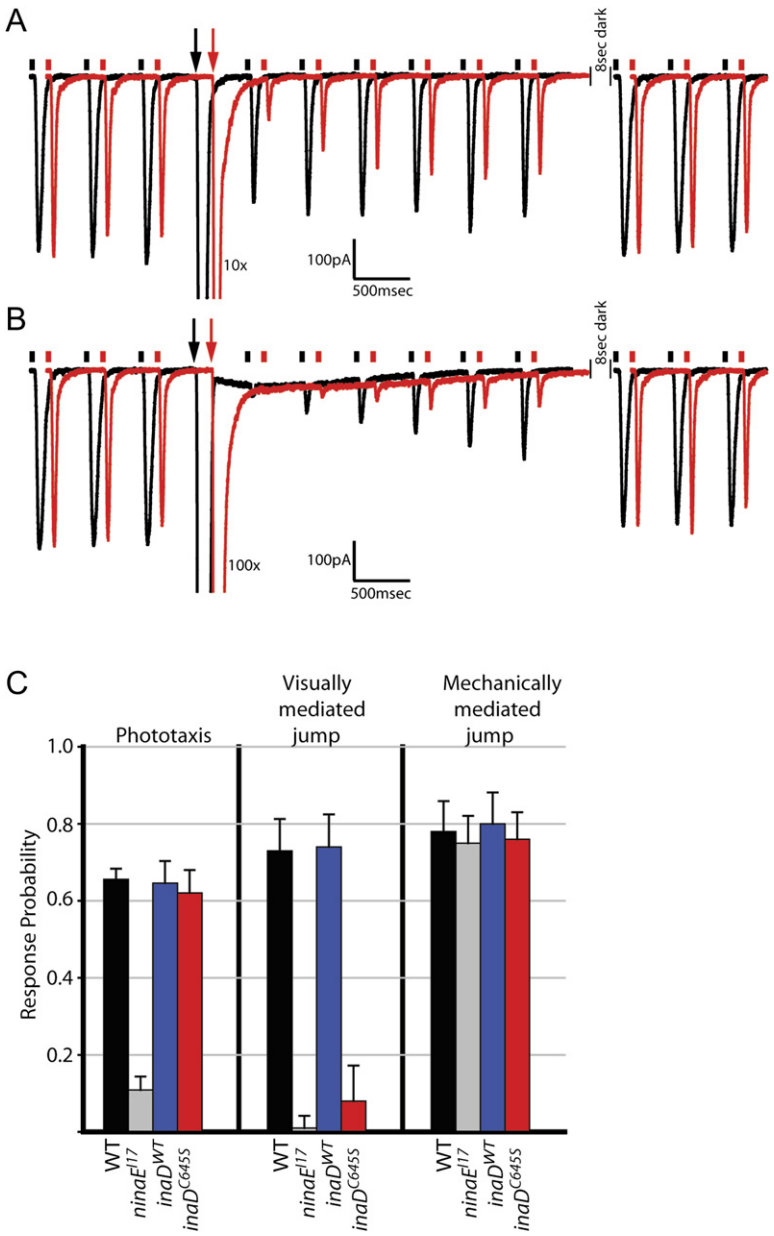

Figure 7. Response Compression and Escape Behavior in *inaD*^{C645S} Flies

(A) Light responses from wild-type (black) and *inaD*^{C645S} (red) cells in response to weak test flashes (rectangles) before and after an adapting flash (arrow) of 10× higher intensity. *inaD*^{C645S} responses are shifted relative to wild-type for clarity.

(B) Same as (A), except the adapting flash (arrow) is 100× higher intensity than the test flashes.

(C) Response probabilities of individual flies in three kinds of behavioral tasks: (left) phototaxis, which measures the ability of flies to walk toward a light source; (middle) visually mediated jumps, which measure the ability of flies to execute an escape jump in response to sudden darkness; (right) mechanically mediated jumps, which measure the ability of flies to execute an escape jump in response to a mechanical shock. Wild-type and *inaD*^{WT} flies perform well on all tasks, while *ninaE*^{I17} flies (null for the major rhodopsin and effectively blind) show defects in both slow and fast timescale visual tasks. *inaD*^{C645S} flies show specific dramatic loss of the visually mediated escape jump (see Movies S1 and S2). Error bars indicate the standard deviations from more than ten individual flies per genotype per task.

tyrosine in *D. melanogaster* and phenylalanine in *C. vicinia* (A. Huber, personal communication). Regardless, the data presented here do support the concept that disulfide exchange dynamics play a key role in *Drosophila* vision.

Induction and Mechanism of the Refractory Period

How does light absorption lead to conformational switching of INAD in vivo? Formation of the PDZ5 disulfide appears to be regulated by a light-dependent protein kinase, eye-PKC, that feedback phosphorylates the INAD scaffold itself. A plausible model is that the light dependence of the INAD conformational switch is due to an allosteric effect within INAD rather than due to a change in environmental redox potential. In this scenario, the redox potential of the PDZ5 disulfide is a function of one or more eye-PKC phosphorylation events in INAD, and the probability of INAD to exist in the oxidized state is set by the relative rates of eye-PKC activity and opposing phosphatase activities. Many other scaffold proteins are known to undergo phosphorylation or other posttranslational modifications to tune pathway output (Bhattacharyya et al., 2006a; Lonart et al., 2003). Work on INAD phosphorylation and its role in controlling PDZ5 structure and function may contribute a model for understanding feedback regulation of scaffolding proteins in general.

How does transient formation of the PDZ5 disulfide mechanistically lead to a refractory period? Genetic studies have demonstrated a role for PDZ5 in controlling the

rhabdomeric localization of PLC-β, the main effector molecule for visual transduction and a component of the INAD complex (Tsunoda et al., 1997). This leads to the obvious hypothesis that light-dependent transient formation of the oxidized state causes transient unbinding (and mislocalization) of PLC-β from the INAD complex. Because PLC-β localization is known to be required for efficient visual signaling, it follows that this brief unbinding event might represent the physical basis for the refractory period. However, evidence for direct interaction between INAD-PDZ5 and PLC-β remains elusive (P.M., M.W., and R.R., unpublished data), and the possibility exists that other target proteins in the visual signaling pathway might associate with PDZ5. Future work in identifying and characterizing real-time localization of PDZ5's binding partners in vivo will be required to address this issue.

Potential Evolutionary Implications

While the core features of the rhodopsin-Gq-PLC-PKC-TRP visual signaling pathway appear to be conserved from insects to mammals, the PDZ5 disulfide appears to be present only in the *Brachycera* suborder of flies. This suborder is specific to the fast-flying insects; other flies (e.g., the *Nematocera* suborder, including *Anopheles* and *Aedes*) display mostly sluggish flying behavior and are nocturnal (Laughlin and Weckstrom, 1993); in addition, they have structurally distinct photoreceptors (Seifert and Smolua, 1990) and do not possess cysteines 606 and 645 in their scaffolding protein. We suspect that use of the PDZ5 disulfide offers a specific advantage to flight at fast speeds where high-frequency visual signals must be processed into aerodynamic decisions. The invertebrate eye has been shown to be an extremely evolvable system with specialization occurring at the family and species level, and even between different sexes of the same species (Franceschini et al., 1981; Laughlin and Weckstrom, 1993; O'Carroll et al., 1996). A scaffolding protein, which coordinates the organization of the key signaling components, seems ideally suited to serve as a "control" center for the system. Modification of scaffolds may represent an attractive mechanism for evolving new features into a signaling pathway without changing its core constituents.

EXPERIMENTAL PROCEDURES

Protein Crystallization and Structure Determination

PDZ5 (residues 580–665 from *D. melanogaster* INAD) was expressed as a GST fusion in *E. coli* BL21-DE3 cells (Stratagene) and subjected to glutathione affinity chromatography, cleavage of the GST tag by 1:50 w/w Factor Xa protease (GE), size exclusion chromatography, and concentration into 50 mM Tris, 100 mM NaCl (pH 7.5). For the reduced state structure, buffers were supplemented with 1 mM DTT during size-exclusion chromatography. Selenomethionyl (SeMet) protein was produced for the reduced and C645S structures by growing cells in M9 minimal media at 37°C to OD_{600} of 1.0, then incubating with amino acids (lysine, phenylalanine, threonine at 100 mg/l; isoleucine, leucine, valine at 50 mg/l; Se-methionine at 60 mg/l). Purified PDZ5 was concentrated to 15 mg/ml without (oxidized and C645S structures) or with (reduced structure) 10 mM DTT, and crystallization trials were conducted at 4°C using the vapor diffusion hanging drop method. Crystals grew either spontaneously or with microseeding with well solutions containing 1.3 M NaCitrate (pH 7.5) in 1–3 days. Single crystals were cryoprotected by serial equilibration into well solutions containing increasing amounts of glycerol (up to 15%) and flash frozen in liquid propane. For the oxidized structure, heavy-atom derivatives were obtained by soaking single crystals in well solution containing either K_2PtCl_4 (1 mM) or trans-$Pd(NH_3)_2Cl_2$ (2.5 mM) for 1 to 2 days prior to cryoprotection.

Data were collected at 100 K and were indexed and scaled with DENZO/SCALEPACK. All phasing and model refinement was carried out without noncrystallographic symmetry restraints using the crystallography and NMR system (CNS) software, and the statistics are summarized in Tables S1–S3. Manual model building was performed in O, and computational refinement steps involved high-temperature torsion angle molecular dynamics followed by positional and temperature factor minimization. Details regarding structure determination are presented in the Supplemental Experimental Procedures. The atomic coordinates have been deposited in the Protein Data Bank with the following accession codes: 2QKT (0 mM DTT), 2QKU (10 mM DTT), and 2QKV (C645S).

Cysteine-Labeling Assays

For in vitro assays, reactions were carried out with purified PDZ5 in 10 mM HEPES and 50 mM NaCl (pH 7.0) and supplemented with various amounts of DTT. All buffers and tubes were flushed with N_2. After incubation for 4 hr at 30°C to reach equilibrium (Figure S6), reactions were quenched with the addition of cold trichloroacetic acid (TCA) to 25% and precipitated on ice for >1 hr. The pellet was collected by centrifugation at 13,000 × g, washed with acetone and resolubilized in 1% SDS, 200 mM Na_2HPO_4 (pH 7.0) supplemented with 20 mM 4-acetamido-4′-maleimidystilbene-2,2′-disulfonic acid (AMS; MW, 536.44 Da; Molecular Probes). The labeling reaction proceeded for 10 min at room temperature and was directly loaded onto a 16.5% Tris-Tricine gel (Bio-Rad). Protein was visualized by Coomassie staining and was imaged and quantified on an AlphaImager HP (AlphaInnotech). Standard redox potentials at 30°C (pH 7) were calculated in triplicate as described previously (Hanson et al., 2004) using $E'_{0(DTT)} = -0.323V$ (Sajewski and Whitesides, 1980).

For in vivo assays, 1-day-old flies were frozen in liquid N_2 and dehydrated in acetone; retina were dissected and homogenized into PBS supplemented with 25% TCA. Protein was collected and washed as above, and resolubilized in denaturing buffer (8 M urea, 100 mM HEPES, and 2% CHAPS [pH 7.0]) + 20 mM AMS. The reaction was quenched after 10 min by addition of TCA to 25%. After precipitation on ice, the pellet was collected, washed, resolubilized in denaturing buffer + 10 mM Tris(2-carboxyethyl)phosphine (TCEP), and incubated for 1 hr to reduce disulfide bonds. Cy3 maleimide (GE) was then added to 10 mM; the reaction was quenched after 10 min by addition of TCA to 25%, and the protein was precipitated and collected as before. The pellet was resolubilized in 8 M urea, 2% CHAPS, 2% IPG buffer pH3–10 (GE) and loaded onto a Immobiline DryStrip pH3–10 linear gel (GE) for electrofocusing, followed by SDS-PAGE on a 10% Tris-HCl gel (Bio-Rad). The gel was directly imaged on a Typhoon 9210 (GE) with excitation at 532 nM and detection at 580 nm. Gels were then fixed and stained for total protein using SYPRO ruby stain (Molecular Probes), and imaged on an AlphaImager HP (AlphaInnotech).

Antibodies

Polyclonal rabbit antibodies to INAD were generated (Covance) using purified recombinant first PDZ domain of INAD (PDZ1) as antigen, and to Arr2 using a synthetic peptide (residues 370–380) as antigen. Sera from immunized rabbits were affinity purified using standard procedures.

Electrophysiology

Whole-cell path clamp on isolated photoreceptors was performed as described previously (Ranganathan et al., 1991). Briefly, retinas from

dark-reared flies were dissected under dim red light in 125 mM $CsCl_2$, 10 mM HEPES, and 30 mM sucrose (pH 7.1) and gently triturated into bath solution (120 mM NaCl, 5 mM KCl, 10 mM HEPES, 4 mM $MgCl_2$, 24 mM proline, 5 mM alanine, and 1.5 mM $CaCl_2$ [pH7.1]). Electrode solution was 140 mM K-gluconate, 10 mM HEPES, 2 mM $MgSO_4$, 1 mM NAD, 4 mM MgATP, 0.5 mM NaGTP, and 0.5 mM EGTA (pH 7.1). Reversal potentials were between −40 and −70 mV; series resistance was typically 10–20 MΩ and was routinely compensated to 75%. No series compensation was used during quantum bump recordings. Signals were amplified with an Axopatch 200B (Axon Instruments), filtered at 100 or 200 Hz (LPF-8, Warner Instrument), and digitized at 10 kHz (PCI-6052E DAQ board [National Instruments]) for analysis.

Light responses were elicited by a 3 ns flash of 580 nm light from a dye-stirred VSL-337-ND-S nitrogen laser (Laser Science). Unattenuated intensity corresponds to $\sim 10^4$ effective photons per flash; light was filtered using neutral density filters (Oriel). Thirty hertz stimulation was used to measure the sensitivity threshold (Figure 5H). Light responses for the stationary fluctuation analysis (Figures 6C–6E) and synchronization experiments (Figures 6H and 6I) were elicited with constant white light from a Xenon arc lamp (Lambda LS [Sutter]; unattenuated intensity ~60 lux), fitted with a *Smart*Shutter (Sutter), and filtered using neutral density filters (Oriel).

Quantum bumps were collected using laser flashes at intensities that generated responses at less than 30% success rate; typically $\log(I/I_0) < -5.0$. Latencies were calculated by hand and used to align bumps. Average bump shapes were calculated by averaging >50 aligned and normalized bumps per genotype. For macroscopic recordings, numerous responses (n = 10) were collected at each light intensity from multiple cells (n > 3). For stationary fluctuation analysis, recordings were performed in n > 4 cells per genotype; analysis was performed as previously described (Johnson and Pak, 1986; Juusola and Hardie, 2001; Wu and Pak, 1978) (see Supplemental Experimental Procedures for details).

Behavioral Assays

All assays were performed on flies less than 1 day old. Phototaxis was tested using the countercurrent apparatus (Benzer, 1967); groups of 25 flies were given a choice between a vial facing a light source (provided by a green light-emitting diode [LED]) and a vial facing away from the light source. Each fly was given the choice eight times.

For the visually mediated escape jump, individual flies were tested in a small Petri dish illuminated with four green LEDs placed at 90° to one another (total intensity, ~80 lux). A "lights-off" stimulus was provided by turning the LEDs off for 20 ms using a TTL signal; escape jumps were monitored visually and recorded. For a mechanical stimulus, the Petri dish was dropped onto a table from a height of 1 cm; escape jumps were monitored visually and recorded. Each fly received ten trials of each stimulus.

Supplemental Data

Supplemental Data include Supplemental Experimental Procedures, Supplemental References, four tables, six figures, and two movies and can be found with this article online at http://www.cell.com/cgi/content/full/131/1/80/DC1/.

ACKNOWLEDGMENTS

We thank F. El-Mazouni, D. DeCamp, and M. Mumby for assistance with 2D gel electrophoresis; A. Fayyazuddin and P. Heisinger for assistance with behavioral assays; A. Huber for communication of unpublished data; and D. Benavides, E. Kavalali, H. Lee, T. Rand, and E. Ross for critical reading of the manuscript. We acknowledge support from the UT Southwestern Medical Scientist Training Program and the Graduate School (P.M. and J.G.) and support from the Robert A. Welch Foundation (R.R.). R.R. is an investigator of the Howard Hughes Medical Institute.

Received: January 16, 2007
Revised: June 7, 2007
Accepted: July 19, 2007
Published: October 4, 2007

REFERENCES

Bauman, A.L., Soughayer, J., Nguyen, B.T., Willoughby, D., Carnegie, G.K., Wong, W., Hoshi, N., Langeberg, L.K., Cooper, D.M., Dessauer, C.W., and Scott, J.D. (2006). Dynamic regulation of cAMP synthesis through anchored PKA-adenylyl cyclase V/VI complexes. Mol. Cell *23*, 925–931.

Benzer, S. (1967). Behavioral mutants of Drosophila isolated by countercurrent distribution. Proc. Natl. Acad. Sci. USA *58*, 1112–1119.

Bhattacharyya, R.P., Remenyi, A., Good, M.C., Bashor, C.J., Falick, A.M., and Lim, W.A. (2006a). The Ste5 scaffold allosterically modulates signaling output of the yeast mating pathway. Science *311*, 822–826.

Bhattacharyya, R.P., Remenyi, A., Yeh, B.J., and Lim, W.A. (2006b). Domains, motifs, and scaffolds: the role of modular interactions in the evolution and wiring of cell signaling circuits. Annu. Rev. Biochem. *75*, 655–680.

Bloomquist, B.T., Shortridge, R.D., Schneuwly, S., Perdew, M., Montell, C., Steller, H., Rubin, G., and Pak, W.L. (1988). Isolation of a putative phospholipase C gene of Drosophila, norpA, and its role in phototransduction. Cell *54*, 723–733.

Burack, W.R., and Shaw, A.S. (2000). Signal transduction: hanging on a scaffold. Curr. Opin. Cell Biol. *12*, 211–216.

Celniker, S.E., Wheeler, D.A., Kronmiller, B., Carlson, J.W., Halpern, A., Patel, S., Adams, M., Champe, M., Dugan, S.P., Frise, E., et al. (2002). Finishing a whole-genome shotgun: release 3 of the Drosophila melanogaster euchromatic genome sequence. Genome Biol. *3*, RESEARCH0079.

Chevesich, J., Kreuz, A.J., and Montell, C. (1997). Requirement for the PDZ domain protein, INAD, for localization of the TRP store-operated channel to a signaling complex. Neuron *18*, 95–105.

Dolph, P.J., Ranganathan, R., Colley, N.J., Hardy, R.W., Socolich, M., and Zuker, C.S. (1993). Arrestin function in inactivation of G protein-coupled receptor rhodopsin in vivo. Science *260*, 1910–1916.

Doyle, D.A., Lee, A., Lewis, J., Kim, E., Sheng, M., and MacKinnon, R. (1996). Crystal structures of a complexed and peptide-free membrane protein-binding domain: molecular basis of peptide recognition by PDZ. Cell *85*, 1067–1076.

Franceschini, N., Hardie, R., Ribi, W., and Kirschfeld, K. (1981). Sexual dimorphism in a photoreceptor. Nature *291*, 241–244.

Hanson, G.T., Aggeler, R., Oglesbee, D., Cannon, M., Capaldi, R.A., Tsien, R.Y., and Remington, S.J. (2004). Investigating mitochondrial redox potential with redox-sensitive green fluorescent protein indicators. J. Biol. Chem. *279*, 13044–13053.

Hardie, R.C. (2001). Phototransduction in Drosophila melanogaster. J. Exp. Biol. *204*, 3403–3409.

Hardie, R.C., and Raghu, P. (2001). Visual transduction in Drosophila. Nature *413*, 186–193.

Henderson, S.R., Reuss, H., and Hardie, R.C. (2000). Single photon responses in Drosophila photoreceptors and their regulation by Ca2+. J. Physiol. *524*, 179–194.

Holmqvist, M.H., and Srinivasan, M.V. (1991). A visually evoked escape response of the housefly. J. Comp. Physiol. [A] *169*, 451–459.

Huber, A. (2001). Scaffolding proteins organize multimolecular protein complexes for sensory signal transduction. Eur. J. Neurosci. *14*, 769–776.

Huber, A., Sander, P., Gobert, A., Bahner, M., Hermann, R., and Paulsen, R. (1996). The transient receptor potential protein (Trp),

a putative store-operated Ca2+ channel essential for phosphoinositide-mediated photoreception, forms a signaling complex with NorpA, InaC and InaD. EMBO J. *15*, 7036–7045.

Hung, A.Y., and Sheng, M. (2002). PDZ domains: structural modules for protein complex assembly. J. Biol. Chem. *277*, 5699–5702.

Hwang, C., Lodish, H.F., and Sinskey, A.J. (1995). Measurement of glutathione redox state in cytosol and secretory pathway of cultured cells. Methods Enzymol. *251*, 212–221.

Iakhine, R., Chorna-Ornan, I., Zars, T., Elia, N., Cheng, Y., Selinger, Z., Minke, B., and Hyde, D.R. (2004). Novel dominant rhodopsin mutation triggers two mechanisms of retinal degeneration and photoreceptor desensitization. J. Neurosci. *24*, 2516–2526.

Johnson, E.C., and Pak, W.L. (1986). Electrophysiological study of Drosophila rhodopsin mutants. J. Gen. Physiol. *88*, 651–673.

Juusola, M., and Hardie, R.C. (2001). Light adaptation in Drosophila photoreceptors: I. Response dynamics and signaling efficiency at 25 degrees C. J. Gen. Physiol. *117*, 3–25.

Keese, M.A., Saffrich, R., Dandekar, T., Becker, K., and Schirmer, R.H. (1999). Microinjected glutathione reductase crystals as indicators of the redox status in living cells. FEBS Lett. *447*, 135–138.

Kimple, M.E., Siderovski, D.P., and Sondek, J. (2001). Functional relevance of the disulfide-linked complex of the N-terminal PDZ domain of InaD with NorpA. EMBO J. *20*, 4414–4422.

Laughlin, S.B., and Weckstrom, M. (1993). Fast and slow photoreceptors—a comparative study of the functional diversity of coding and conductances in the Diptera. J. Comp. Physiol. *172*, 593–609.

Leichert, L.I., and Jakob, U. (2004). Protein thiol modifications visualized in vivo. PLoS Biol. *2*, e333. 10.1371/journal.pbio.0020333.

Lonart, G., Schoch, S., Kaeser, P.S., Larkin, C.J., Sudhof, T.C., and Linden, D.J. (2003). Phosphorylation of RIM1alpha by PKA triggers presynaptic long-term potentiation at cerebellar parallel fiber synapses. Cell *115*, 49–60.

Matsumoto, H., Kahn, E.S., and Komori, N. (1999). The emerging role of mass spectrometry in molecular biosciences: studies of protein phosphorylation in fly eyes as an example. Novartis Found. Symp. *224*, 225–244.

Montell, C. (1998). TRP trapped in fly signaling web. Curr. Opin. Neurobiol. *8*, 389–397.

Montell, C. (2005). TRP channels in Drosophila photoreceptor cells. J. Physiol. *567*, 45–51.

Morrison, D.K., and Davis, R.J. (2003). Regulation of MAP kinase signaling modules by scaffold proteins in mammals. Annu. Rev. Cell Dev. Biol. *19*, 91–118.

O'Carroll, D.C., Bidwell, N.J., Laughlin, S.B., and Warrant, E.J. (1996). Insect motion detectors matched to visual ecology. Nature *382*, 63–66.

Ostergaard, H., Tachibana, C., and Winther, J.R. (2004). Monitoring disulfide bond formation in the eukaryotic cytosol. J. Cell Biol. *166*, 337–345.

Popescu, D.C., Ham, A.J., and Shieh, B.H. (2006). Scaffolding protein INAD regulates deactivation of vision by promoting phosphorylation of transient receptor potential by eye protein kinase C in Drosophila. J. Neurosci. *26*, 8570–8577.

Ranganathan, R., Harris, G.L., Stevens, C.F., and Zuker, C.S. (1991). A Drosophila mutant defective in extracellular calcium-dependent photoreceptor deactivation and rapid desensitization. Nature *354*, 230–232.

Sajewski, R.P., and Whitesides, G.M. (1980). Rate constants and equilibrium constants for thiol-disulfide interchange reactions involving oxidized glutathione. J. Am. Chem. Soc. *102*, 2011–2015.

Schoch, S., Castillo, P.E., Jo, T., Mukherjee, K., Geppert, M., Wang, Y., Schmitz, F., Malenka, R.C., and Sudhof, T.C. (2002). RIM1alpha forms a protein scaffold for regulating neurotransmitter release at the active zone. Nature *415*, 321–326.

Scott, K., and Zuker, C.S. (1998). Assembly of the Drosophila phototransduction cascade into a signalling complex shapes elementary responses. Nature *395*, 805–808.

Scott, K., Sun, Y., Beckingham, K., and Zuker, C.S. (1997). Calmodulin regulation of Drosophila light-activated channels and receptor function mediates termination of the light response in vivo. Cell *91*, 375–383.

Seifert, P., and Smolua, U. (1990). Adaptive structural changes indicate an evolutionary progression towards the open rhabdom in diptera. J. Evol. Biol. *3*, 225–242.

Shieh, B.H., and Zhu, M.Y. (1996). Regulation of the TRP Ca2+ channel by INAD in Drosophila photoreceptors. Neuron *16*, 991–998.

Shieh, B.H., Zhu, M.Y., Lee, J.K., Kelly, I.M., and Bahiraei, F. (1997). Association of INAD with NORPA is essential for controlled activation and deactivation of Drosophila phototransduction in vivo. Proc. Natl. Acad. Sci. USA *94*, 12682–12687.

Smith, D.P., Ranganathan, R., Hardy, R.W., Marx, J., Tsuchida, T., and Zuker, C.S. (1991). Photoreceptor deactivation and retinal degeneration mediated by a photoreceptor-specific protein kinase C. Science *254*, 1478–1484.

Tsunoda, S., and Zuker, C.S. (1999). The organization of INAD-signaling complexes by a multivalent PDZ domain protein in Drosophila photoreceptor cells ensures sensitivity and speed of signaling. Cell Calcium *26*, 165–171.

Tsunoda, S., Sierralta, J., Sun, Y., Bodner, R., Suzuki, E., Becker, A., Socolich, M., and Zuker, C.S. (1997). A multivalent PDZ-domain protein assembles signalling complexes in a G-protein-coupled cascade. Nature *388*, 243–249.

Wong, F., and Knight, B.W. (1980). Adapting-bump model for eccentric cells of Limulus. J. Gen. Physiol. *76*, 539–557.

Wong, W., and Scott, J.D. (2004). AKAP signalling complexes: focal points in space and time. Nat. Rev. Mol. Cell Biol. *5*, 959–970.

Wu, C.F., and Pak, W.L. (1978). Light-induced voltage noise in the photoreceptor of Drosophila melanogaster. J. Gen. Physiol. *71*, 249–268.

Wyman, R.J., Thomas, J.B., Salkoff, L., and King, D.G. (1984). The Drosophila giant fiber system. In Neural Mechanisms of Startle Behavior, R.C. Eaton, ed. (New York:: Plenum Press), pp. 133–161.

Accession Numbers

The PDB accession numbers for the structures reported in this paper are 2QKT, 2QKU, and 2QKV.